Two-dimensional quantitative photoacoustic image reconstruction of absorption distributions in scattering media by use of a simple iterative method

Benjamin T. Cox, Simon R. Arridge, Kornel P. Köstli, and Paul C. Beard

Photoacoustic imaging is a noninvasive biomedical imaging modality for visualizing the internal structure and function of soft tissues. Conventionally, an image proportional to the absorbed optical energy is reconstructed from measurements of light-induced acoustic emissions. We describe a simple iterative algorithm to recover the distribution of optical absorption coefficients from the image of the absorbed optical energy. The algorithm, which incorporates a diffusion-based finite-element model of light transport, converges quickly onto an accurate estimate of the distribution of absolute absorption coefficients. Two-dimensional examples with physiologically realistic optical properties are shown. The ability to recover optical properties (which directly reflect tissue physiology) could enhance photoacoustic imaging techniques, particularly methods based on spectroscopic analysis of chromophores.

OCIS codes: 110.5120, 170.5120.

1. Introduction

Biomedical photoacoustic (PA) imaging provides a means of visualizing the internal structure and function of soft tissues. The image contrast is provided by light-absorbing chromophores within the tissue. These may be naturally occuring, such as oxyhemoglobin and deoxyhemoglobin, or externally administered, e.g., dyes, nanoparticles, or other contrast agents. In conventional PA imaging, the spatially varying pressure increase following the absorption of a laser pulse is reconstructed from time-resolved measurements of the subsequent acoustic radiation recorded over the tissue surface.[1–3] Assuming impulsive deposition of the laser energy and acoustic homogeneity, this image of the initial pressure distribution is proportional to the absorbed optical energy density. Because the absorbed energy density is the product of both the absorption coefficient and the fluence, this image has the disadvantage that it provides a somewhat indirect representation of the spatial variation of the optical coefficients and therefore the structure and physiology of the tissue. In this paper, we address this by recovering the spatial distribution of the optical absorption coefficient from the absorbed optical energy by using an iteratively applied forward model of light transport. Because this produces a map of the optical absorption coefficient in absolute units, it is referred to as quantitative PA imaging.

There are several important advantages to obtaining an image of the absorption coefficient distribution rather than the absorbed optical energy. The absorption coefficient distribution, unlike the absorbed energy map, is directly related to the spatial distribution of absorbing chromophores in the tissue and does not depend on the light fluence. This provides for a truer image contrast distribution and therefore aids the visual interpretation of the image—most obviously, for example, it removes the depth-dependent falloff in contrast that is due to optical attenuation. Important as this is, particularly when one is interpreting images of complex anatomical structures, its greatest significance lies in spectroscopic imaging. Here the objective is to quantify the concentration of specific chromophores, perhaps endogenous, such as oxyhemoglobin and deoxyhemoglobin for the measurement of blood oxygenation,[4–6] or exogeneous contrast agents, such as those proposed for use in PA molecular imaging applications,[7] by means of their known spectral signatures. Obtaining the latter directly from mul-

B. T. Cox (bencox@medphys.ucl.ac.uk), K. P. Köstli, and P. C. Beard are with the Department of Medical Physics and Bioengineering, University College London, Gower Street, London WC1E 6BT, UK. S. R. Arridge is with the Department of Computer Science, University College London, Gower Street, London WC1E 6BT, UK.

Received 28 June 2005; accepted 15 August 2005; posted 27 September 2005 (Doc. ID 63074).

0003-6935/06/081866-09$15.00/0

tiwavelength images of the absorbed energy can be problematic because the wavelength dependence at any point is, in effect, encoded with the spectral characteristics of all the chromophores throughout the illuminated tissue volume. The effect of such spatial-spectroscopic cross talk is to corrupt the spectral signature of the chromophore of interest, seriously compromising the ability to identify its presence and quantify its concentration. Reconstructing images in terms of the absolute absorption coefficient at multiple wavelengths avoids this. Finally, because the image is quantitatively reconstructed in units of optical absorption, it offers the prospect of making comparisons over time of absolute changes in physiological parameters.

Relatively little work has been done in this area, despite its obvious advantages. Methods for estimating the depth-dependent absorption in a layered medium from a PA time series measured in the acoustic far and near fields have been described,[8–10] but they are limited to the one-dimensional case and nonscattering media. The Born approximation was used in an inversion scheme for small perturbations in the absorption coefficient distribution over a known background absorption in an infinite, homogeneous, scattering medium, when both the scattering and background absorption coefficients are known.[11] It provides a good estimate of the heterogeneous optical absorption coefficient distribution when the light fluence distribution that is due to the background absorption is changed little by the absorption perturbations, i.e., for low absorption perturbations.

In this paper we describe a simple iterative method for estimating arbitrary two-dimensional (2D) absorption coefficient distributions quantitatively from the absorbed energy map in a scattering medium. In Section 2 we review the principle of conventional PA imaging, in which the image is a combination of the absorption coefficient distribution and the fluence. In Section 3 we describe a method for removing the effect of the fluence from the image, leaving just an image of the absorption coefficient distribution, by using a forward model of light transport (Subsection 3.A) in a recursive algorithm (Subsection 3.B). Several examples that use simulated measurements are described in Section 4, demonstrating that the technique can recover arbitrary absorption distributions from measurements containing noise.

2. Photoacoustic Imaging: Reconstructing for the Absorbed Energy Distribution

If a region of a fluid is heated through the absorption of a laser pulse, a sound wave is generated. In a stationary fluid with isotropic acoustic properties, under conditions whereby the sound-generation mechanism is thermoelastic, the effects of viscosity and thermal conductivity can be neglected (thermal confinement), and linear propagation can be assumed, the wave equation for the acoustic pressure p is[12,13]

$$\nabla^2 p - \frac{1}{c^2}\frac{\partial^2 p}{\partial t^2} = \frac{-\beta}{C_p}\frac{\partial \mathcal{H}}{\partial t}, \tag{1}$$

where c is the sound speed, β is the volume thermal expansivity, C_p is the constant-pressure specific-heat capacity, and $\mathcal{H}$ is the heat energy per unit volume and per unit time deposited in the fluid. p and $\mathcal{H}$ will depend, in general, on the position $\mathbf{r} = (x, y, z)$ and time t. When the laser pulse is sufficiently short that the optical energy is absorbed before the fluid density has time to change (stress confinement[14]), the heating function can be modeled as a δ function in time,

$$\mathcal{H}(\mathbf{r}, t) = H(\mathbf{r})\delta(t), \tag{2}$$

where $H(\mathbf{r})$ is the heat deposited in the fluid per unit volume because of the absorbed laser energy. If the absorption coefficient distribution at a point in the fluid is $\mu_a(\mathbf{r})$ and the light fluence is $\Phi(\mathbf{r}; \mu_a)$, then the spatial part of the heating function can be written as

$$H(\mathbf{r}) = \mu_a(\mathbf{r})\Phi(\mathbf{r}; \mu_a). \tag{3}$$

The deposited energy density or spatial heating function, $H(\mathbf{r})$, is termed the absorbed energy map because it represents the distribution of absorbed optical energy. As the fluence $\Phi(\mathbf{r})$ will in general depend on the absorption coefficient distribution $\mu_a(\mathbf{r})$, as well as on the scattering coefficient distribution $\mu_s(\mathbf{r})$ and the anisotropy factor $g(\mathbf{r})$, the absorbed energy H is noninearly related to μ_a. In the case of δ-function heating, Eq. (2), the acoustic pressure immediately following the laser pulse, or initial pressure distribution, $p_0(\mathbf{r})$, is proportional to the absorbed energy map,

$$p_0(\mathbf{r}) = \left(\frac{\beta c^2}{C_p}\right)H(\mathbf{r}) = \Gamma H(\mathbf{r}), \tag{4}$$

where Γ is the Grüneisen coefficient, a dimensionless constant that represents the efficiency of the conversion of heat to pressure. ($\Gamma \approx 0.11$ for water at room temperature.[14]) This initial pressure distribution then propagates away as acoustic waves according to Eq. (1). In biomedical PA imaging these acoustic waves are measured at the tissue surface as a function of time, and backpropagation algorithms are used to obtain an image proportional to the initial pressure distribution p_0 and consequently the absorbed energy map.[1–3,15,16] This map, referred to here as the measured absorbed energy $\hat{H}$, is conventionally called a PA image.

The final step in the image reconstruction process might then be regarded as one in which a model of light transport is fitted to $\hat{H}$ to obtain a quantitative image of the tissue optical properties. It is our objective in this paper to demonstrate this step, so we make the reasonable assumption that p_0, and hence $\hat{H}$, has been reconstructed from the acoustic measure-

ments accurately and with negligible structural distortion. This is discussed in Section 5.

3. Fitting a Model of Light Transport to the Absorbed Energy Distribution

Inverse problems in which unknown parameters must be extracted from measurements of a related quantity are often solved by adjustment of the parameters in a model of the corresponding forward problem until its solution matches the measurements. Here, we solve the inverse problem of estimating the absorption coefficient distribution by adjusting μ_a in a forward model of light transport until it fits a measured absorbed energy distribution. We do this by using a simple fixed-point iteration.

A. Forward Models of Light Transport

An appropriate forward model must be able to calculate the absorbed energy density distribution in a scattering medium, given an arbitrary absorption distribution as a parameter, and, because several iterations may be required for finding the solution, must be able to calculate it quickly. As we assume δ-function heating, Eq. (2), a time-independent light-propagation model is sufficient.

Although Monte Carlo (MC) models provide a reliable and accurate way to calculate light transport in turbid media,[17] they are unsuitable as the forward model in this inverse problem because the geometry of absorption and scattering inhomogeneities must be encoded directly and they are slow to converge. Other numerical methods may be found that satisfy both criteria. A finite-element (FE) model of light transport based on the $P1$ (diffusion) approximation to the transport equation was chosen for this study. Such models are well established in inverse schemes for optical tomography[18,19] because of their accuracy and speed. The $P1$ approximation is valid when $\mu_a \ll \mu_s$ and for distances inside scattering tissue significantly greater than $1/\mu_t$, where $\mu_t = \mu_a + \mu_s$ is the total attenuation coefficient. There may be occasions in biomedical PA imaging when the conditions do not hold, such as when one is imaging superficial targets close to the surface of the scattering medium. To account for this case, a simple adjustment to the scattering parameters in the $P1$ model, based on consideration of the δ-Eddington phase function, was used to more accurately model the fluence at short distances inside the scattering medium.[5,20] The $P1$ approximation assumes almost isotropic radiance, which is not the case close to the tissue surface, where the light from an incident collimated beam remains highly directed. At depths much greater than $1/\mu_t$, where the $P1$ approximation is accurate, the fluence depends on only the reduced scattering coefficient $\mu_s' = \mu_s(1 - g)$ and not on μ_s and g separately. When the scattering coefficient is reduced by a factor of f to $\mu_s(1 - f)$ and the new anisotropy factor is chosen to be $(g - f)/(1 - f)$ (so that μ_s' remains the same), more of the incident light remains unscattered close to the surface, as required, but the solution at depths much greater than $1/\mu_t$ remains unchanged. Following comparisons with MC models, the fraction f was found to be well approximated by $f = g^3$ for the range of optical coefficients used here. The $P1$ approximation, with these modified scattering coefficients, was encoded into a FE model by use of the Galerkin method with a Robin boundary condition[18,19] on a uniform rectangular mesh.

Although we have been discussing a FE model based on the diffusion equation, and we use it throughout the paper, the recursive inversion algorithm described below is not necessarily restricted to using this FE model but could use a FE model based on a higher-order approximation to the transport equation or, indeed, any other suitably efficient model of light transport in turbid media that can accept an arbitrary absorption distribution as a parameter.

B. Recursive Algorithm for Quantitative Estimation of Absorption Coefficient Distributions

In general, the absorbed energy H depends on both the absorption and the scattering coefficients. In Eq. (3), H does not depend explicitly on the scattering but rather depends on it implicitly through the fluence distribution Φ; reconstructing for the scattering would therefore require fitting to a model for the fluence. This, however, is likely to suffer from the nonuniqueness problem identified by Arridge and Lionheart.[21] There are several possible approaches to addressing this issue, such as incorporating prior information about, or constraints on, the scattering distribution, the simplest being to assume that the scattering is constant over the reconstructed volume. This may be reasonable for soft tissues such as postmenopausal breast, liver, and subcutaneous fat, especially when imaging small volumes. Because our main purpose in this paper is to show that a recursive algorithm can quickly recover the absorption coefficient distribution in examples with realistic geometric and optical properties, we make this simplifying assumption and assume that the scattering is known *a priori*. A similar assumption was made by Ripoll and Ntziachristos,[11] as well as in early work in diffuse optical imaging.[21]

If the measured absorbed energy distribution $\hat{H}$, the illumination geometry, and the scattering distribution are known, then the absorption coefficient distribution may be recovered iteratively as follows: (1) The initial estimate for the absorption is set at zero, $\mu_a^{(0)} = 0$; (2) the fluence $\Phi^{(0)}$ that would result from an absorption distribution of $\mu_a^{(0)}$ is calculated with a forward model of the propagation of light in a scattering medium; (3) a new absorption estimate is calculated from $\mu_a^{(1)} = \hat{H}/\Phi^{(0)}$; and (4) calculations of $\Phi^{(k)}$ and $\mu_a^{(k)}$ are iterated until the error in the absorbed energy, $\Delta H^{(k)} = \hat{H} - \mu_a^{(k)}\Phi^{(k)}$, is sufficiently small. This algorithm is shown as a flow chart in Fig. 1 and summarized below.

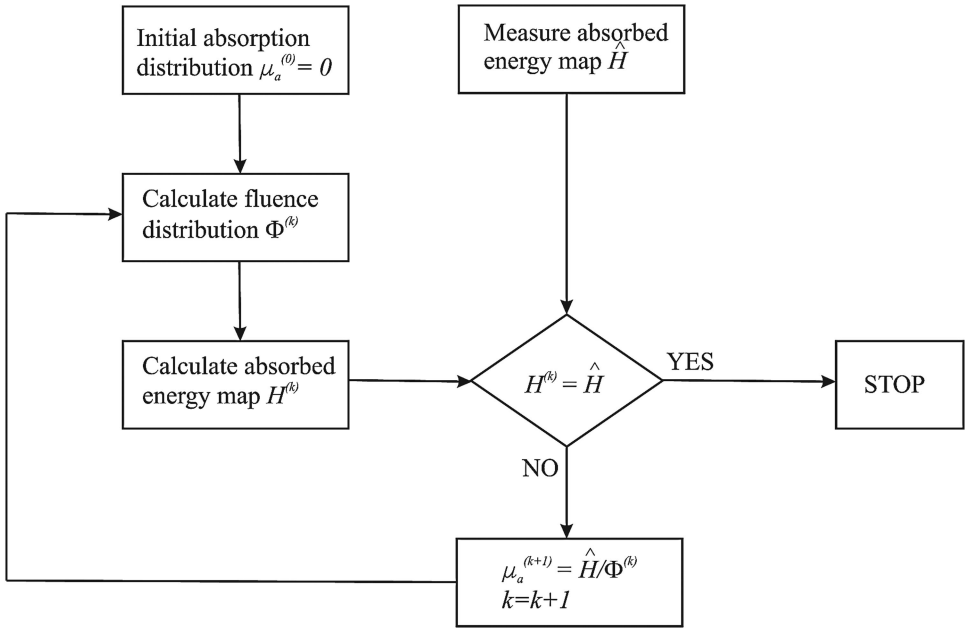

Fig. 1. Flow chart showing the recursive algorithm for quantitative PA imaging.

Quantitative PA imaging algorithm:

$\hat{H}$ has been measured
set stopping criterion ϵ

$\mu_a^{(0)} = 0$
$k = 0$

while $\|\Delta H^{(k)}\| > \epsilon$
calculate fluence $\Phi^{(k)}$ using a forward model
$\Delta H^{(k)} = \hat{H} - \mu_a^{(k)}\Phi^{(k)}$
$\mu_a^{(k+1)} = \hat{H}/\Phi^{(k)}$
$k = k + 1$

end

Here μ_a, Φ, and $\hat{H}$ are all nonnegative and in $\mathbb{R}^{N^2}$, where N^2 is the number of pixels in the image. It has been shown elsewhere that this iterative algorithm converges to within machine precision of the true absorption in the noise-free case without regularization.[23] However, the estimate of the absorption is more sensitive to errors in the estimate of the fluence, wherever the fluence is low, which can cause instabilities when the measurements contain noise. To see this we differentiate $\mu_a = \hat{H}/\Phi$ to get

$$\frac{\partial \mu_a}{\partial \Phi} = -\frac{\hat{H}}{\Phi^2}, \tag{5}$$

and we note that, at points where Φ is small, $\partial\mu_a/\partial\Phi$ will be large. This potential cause of instability can be dealt with in a number of ways. If the inversion can be restricted to a region of the tissue where the fluence is never low, the instability will not arise. This, however, requires the fluence to be known, at least approximately, in advance, which will not necessarily be the case. A more general approach is to add a positive regularization parameter σ to the denominator and calculate the absorption update by use of

$$\mu_a^{(k+1)} = \frac{\hat{H}}{\Phi^{(k)} + \sigma}. \tag{6}$$

If the measurements are split into the exact absorbed energy H and noise $\mathcal{N}$, so $\hat{H} = H + \mathcal{N}$, then the sensitivity can now be written as two terms,

$$\frac{\partial \mu_a}{\partial \Phi} = -\frac{H}{(\Phi + \sigma)^2} - \frac{\mathcal{N}}{(\Phi + \sigma)^2}, \tag{7}$$

where the effect of the regularization parameter becomes apparent. Increasing σ reduces the sensitivity of the absorption estimate to the noise at the expense of reducing the rate of convergence to the, now approximate, solution $H/(\Phi + \sigma)$. The advantage of this method of regularization is that, in addition to preventing the estimates where the fluence is low from blowing up and corrupting the whole solution, it also does not blur the edges, which represent the sharp changes in absorption. This is in contrast to regularizing the solution by smoothing (i.e., by removing the high-spatial-frequency components on the basis that the required solution varies more smoothly than the noise), which would blur the sharp boundaries throughout the image.

The regularization parameter σ could, in principle, be chosen to be spatially dependent and adjusted before each iteration. It could be proportional to the reciprocal of the spatially dependent signal-to-noise ratio

(SNR), for instance, thereby maximizing the accuracy of the absorption estimate at points where the SNR is large but preventing instability at points where it is too small. For simplicity, we take σ as constant in the examples below. An appropriate value, or values, for σ can be found in a number of ways, for example, by using the L-curve method,[24] or, as we have done in the examples below, by running the inversion several times, increasing σ each time, until no divergence is detected and a stable solution is reached.

4. Numerical Examples

Four examples are provided to demonstrate the above algorithm by recovering the 2D absorption coefficient distribution from simulated measurements of absorbed enery density. In the first example, a 2D MC model of light transport[17] was used to simulate the measured absorbed energy map that would be obtained from a conventional PA reconstruction. For the subsequent examples, with more complex absorption distributions, the MC model was replaced with the FE model described above because of its much greater flexibility and faster run time. Using exactly the same model for the simulation and the reconstruction is considered an inverse crime as the inversion may unwittingly be given *a priori* information that aids the inversion, such as the mesh geometry. To mitigate this inverse crime, the simulated measurements obtained with the FE model were first calculated on a 150×150 mesh and then linearly interpolated to a coarser, noncoincident 71×71 mesh. Noise was added to the simulated data in all the examples. The illumination was chosen to have a top-hat beam profile of 2 mm radius and was incident from left to right. The optical coefficients used are realistic for blood and background tissue in the near-infrared wavelength range.

A. Example Using Data Simulated with the Monte Carlo Model

The first example, which consisted of two rectangular absorbers with absorption coefficients of 0.2 and 0.1 mm^{-1}, within a background absorption of 0.01 mm^{-1}, is shown in Fig. 2A. The scattering coefficient and anisotropy factors were constant, with $\mu_s = 10\ \mathrm{mm}^{-1}$ and $g = 0.8$. The regularization parameter σ was set to 1. The measured absorbed energy map $\hat{H}$, shown in Fig. 2B, was simulated with the 2D MC model. Normally distributed noise was added, and any resulting negative values of $\hat{H}$ were set to zero on the basis that the absorbed energy cannot be negative. The SNR varied from ~40 dB, close to the source, to approximately −10 dB 12 mm away from the surface. Following 20 iterations of the inverse algorithm, the absorption distribution in Fig. 2C was recovered. Horizontal cross sections through the absorption distribution at 3 and −1.5 mm (Fig. 2D) show that the absorption has been recovered well. The final fluence distribution (Fig. 2E) shows that the fluence falls off rapidly with distance from the light source. The effect of this on the absorption coefficient estimate is evident in Fig. 2C, where the noise has corrupted the estimate in the corners far from the source. The squared error, ΔH^2, summed over the region of the inversion is plotted on a log scale as a function of the iteration number in Fig. 2F. As the inversion progresses, the error decreases until the iteration converges. In these inversions, each iteration took <1 s on a personal computer with a 2 GHz processor.

This example shows that the inversion algorithm can be used to obtain an accurate, quantitative estimate of the absorption coefficient distribution from realistic, noisy data that avoid the inverse crime. The inversion converges quickly to an image that shows the structure of the absorbers more clearly and to a greater depth than in the original image of the absorbed energy. Furthermore, the success of the reconstruction is an implicit indication that the FE model agrees with the MC model and is therefore an accurate model of light transport.

B. Example Using Data Simulated with the Finite-Element Model

This example of three absorbers with absorption coefficients of 0.3 mm^{-1} (small circle), 0.2 mm^{-1} (rectangle), and 0.1 mm^{-1} (large circle) is shown in Fig. 3A. The FE model was used to simulate the data. The scattering coefficient, anisotropy factor, and regularization parameter were $\mu_s = 10\ \mathrm{mm}^{-1}$, $g = 0.8$, and $\sigma = 0.1$. The absorption coefficient distribution is shown in Fig. 3A. The simulated data were calculated on a 150×150 mesh and interpolated to a 71×71 mesh to provide the measured $\hat{H}$. Noise was added, as in the previous example, to give a SNR in the range of 40 to −20 dB. The simulated absorbed energy map is shown in Fig. 3B. The downsampling distorts the shape of the small circular absorption inhomogeneity close to the source. The recovered absorption coefficient distribution (Fig. 3C), following 20 iterations, also has a pixelated appearance for the same reason. Nevertheless, good estimates of the absorption coefficient were still recovered. This example shows even more clearly than the previous one the improvement in the image structure following the inversion. The large rectangular absorber is all but invisible in Fig. 3B, but, after the inversion, Fig. 3C is both clear and, except where the fluence is low at the end farthest from the source, quantitatively accurate.

C. Two Contrasting Examples

The final two examples, in Figs. 4 and 5, illustrate that the inversion algorithm is not restricted to recovering specific shapes of absorption inhomogeneities but can recover an arbitrary distribution. Figures 4 and 5 show two contrasting examples, lines, representing a discrete, well-defined structure such as blood vessels, and a more diffuse absorber, representing a target such as a tumor. In both examples the absorbed energy map was simulated with the FE model, downsampled, and noise was added as in the previous example. The scattering coefficient and anisotropy factor were $\mu_s =$

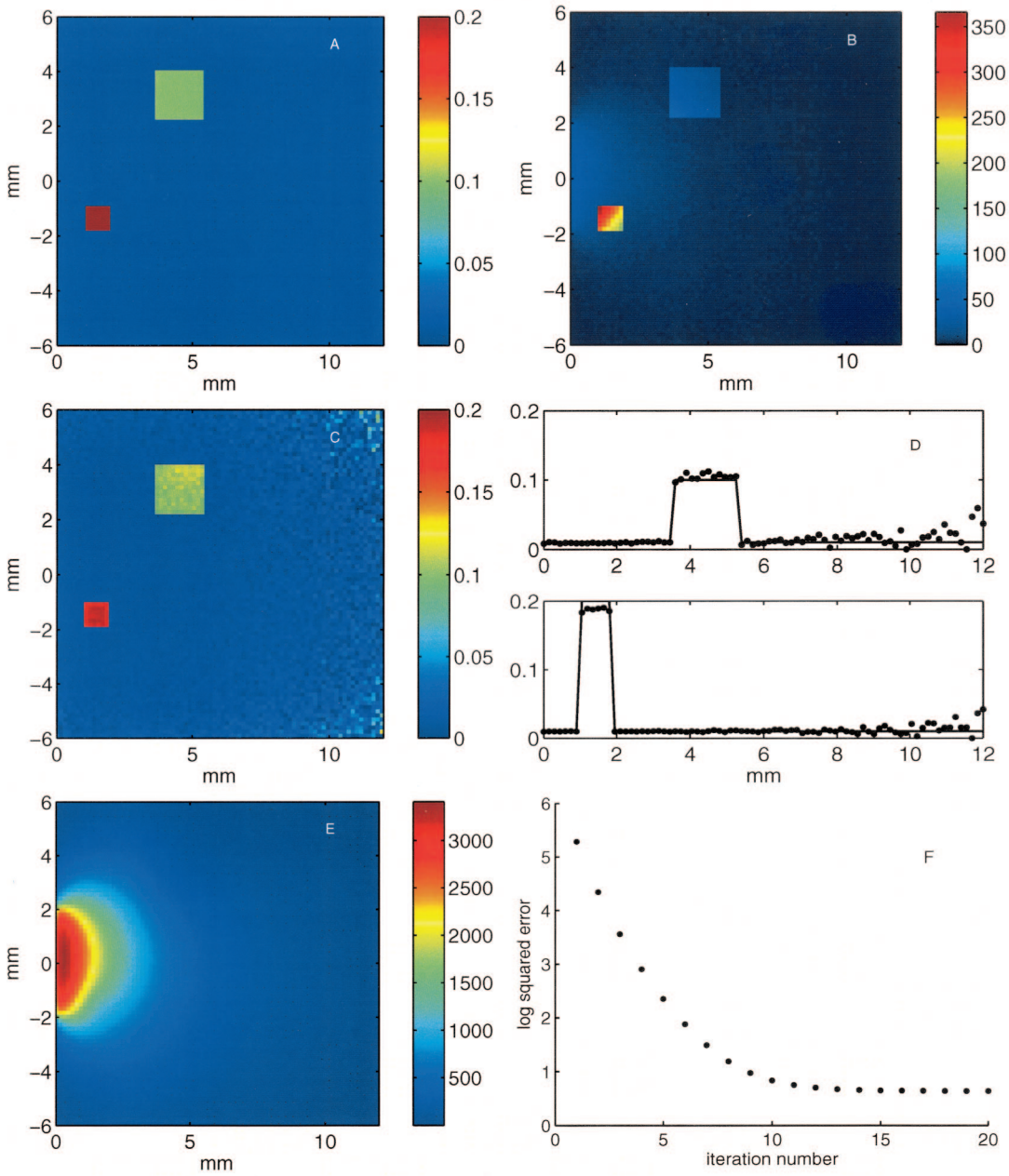

Fig. 2. Quantitative reconstruction of absorbers in a scattering medium by use of data simulated with a MC model. A, true optical absorption distribution with absorption coefficients of 0.2 mm^{-1} (small square), 0.1 mm^{-1} (larger square), and 0.01 mm^{-1} (background). $\mu_s = 10\ mm^{-1}$, $g = 0.8$, $\sigma = 1$. B, measured absorbed energy distribution, in millijoules per cubic centimeter, simulated with a MC model with added noise. The SNR varies across the image from 40 dB, near the light source, to −10 dB farthest away. C, recovered absorption distribution, in inverse millimeters, following 20 iterations. D, horizontal slices through the true (solid) and recovered (dots) absorption distributions at 3 and −1.5 mm. E, recovered fluence, in millijoules per square centimeter, following 20 iterations. F, log (base 10) of the sum of the squared error against iteration number, showing convergence.

10 mm^{-1} and $g = 0.8$, respectively. In Fig. 4, the true absorption coefficient distribution (Fig. 4A) consists of alternating strips of absorption of 0.1 and 0.01 mm^{-1}. In the measured absorbed energy map (Fig. 4B) the striped pattern has been distorted by the fluence distribution, with the stripes fading rapidly with distance from the source both in depth and toward the top and bottom of the image. The recovered absorption (Fig. 4C), with $\sigma = 0.1$, although clearly affected by the noise where the fluence is low, shows that the strips of absorption extend deeper and farther to the sides than the map of absorbed energy suggests. Figure 5 shows an absorption distribution (Fig. 5A) that differs from those considered so far in that it is smooth and continuously changing, without sharp boundaries or regions of constant absorption. The inversion algorithm still recovers a good estimate of the absorption distribution (Fig. 5C) from the ab-

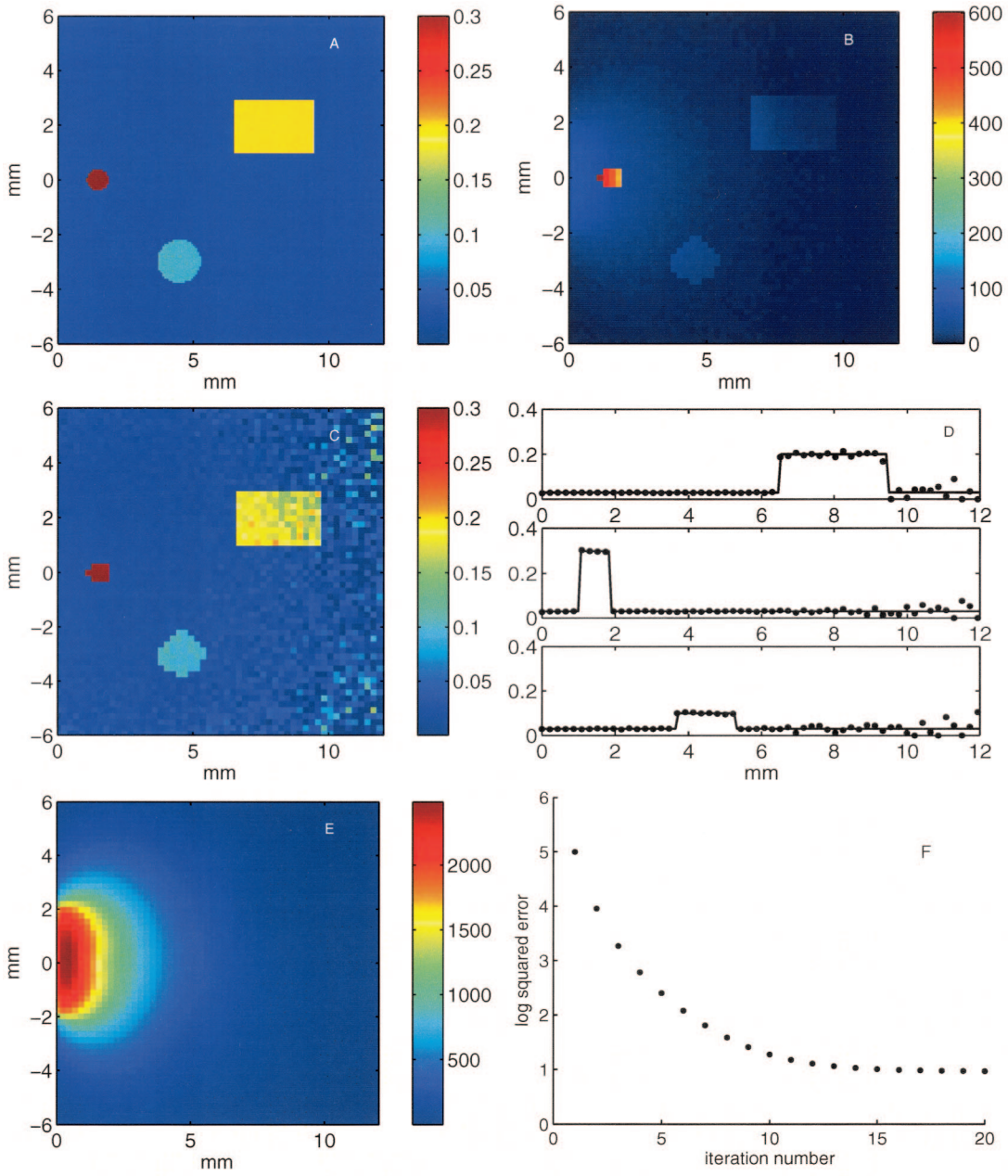

Fig. 3. Quantitative reconstruction of absorbers in a scattering medium by use of data simulated using a FE model. A, true optical absorption distribution with absorption coefficients of 0.3 mm^{-1} (small circle), 0.2 mm^{-1} (square), 0.1 mm^{-1} (larger circle), and 0.01 mm^{-1} (background). $\mu_s = 10\ mm^{-1}$, $g = 0.8$, $\sigma = 0.1$. B, measured absorbed energy distribution, in millijoules per cubic centimeter, simulated with a model. The SNR ranges from 40 to −20 dB. C, recovered absorption distribution, in inverse millimeters, after 20 iterations. D, horizontal slices through the true (solid) and recovered (dots) absorption distributions at 2, 0, and −3 mm. E, recovered fluence, in millijoules per square centimeter, following 20 iterations. F, log (base 10) of the sum of the squared error against iteration number showing convergence.

sorbed energy distribution (Fig. 5B), with $\sigma = 0.1$. The strongest feature in the absorbed energy distribution is a peak close to the point (1, 0). By removal of the distorting effect of the fluence, the peak around (4, −3), where the absorption coefficient is largest, appears as the strongest feature.

5. Discussion

The examples above show that both the structure and good quantitative estimates of the absorption coefficient distribution can be recovered from the absorbed energy map by use of the algorithm described in Subsection 3.B. Obtaining absorption coefficient distributions at many wavelengths will allow chromophores of known spectral characteristics, and thereby physiologically interesting quantities such as blood oxygenation, to be identified and quantified. In PA molecular imaging, in which the abundance of a biomolecule of interest is indicated by the concentration of a marker chromophore, it is

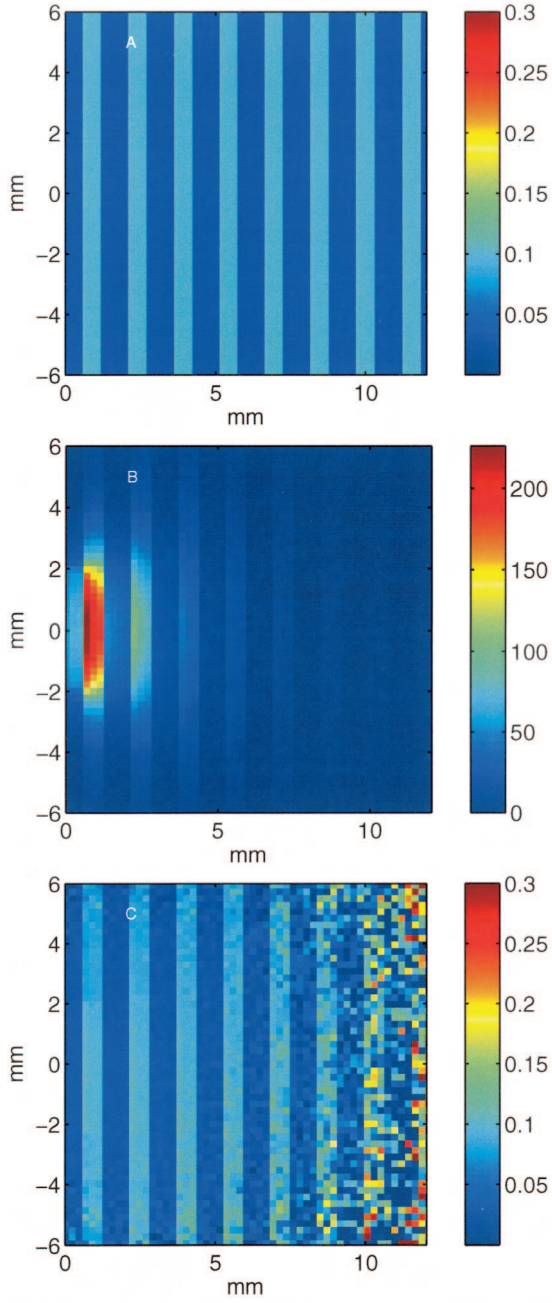

Fig. 4. Quantitative reconstruction of absorbing strips in a scattering medium. A, true absorption distribution consisting of alternate lines with absorption coefficients 0.2 and 0.01 mm^{-1}. μ_s = 10 mm^{-1}, g = 0.8, σ = 0.1. B, measured absorbed energy distribution, in millijoules per cubic centimeter, simulated with a FE model. The SNR ranges from 40 to −20 dB. C, recovered absorption distribution, in inverse millimeters, following 20 iterations.

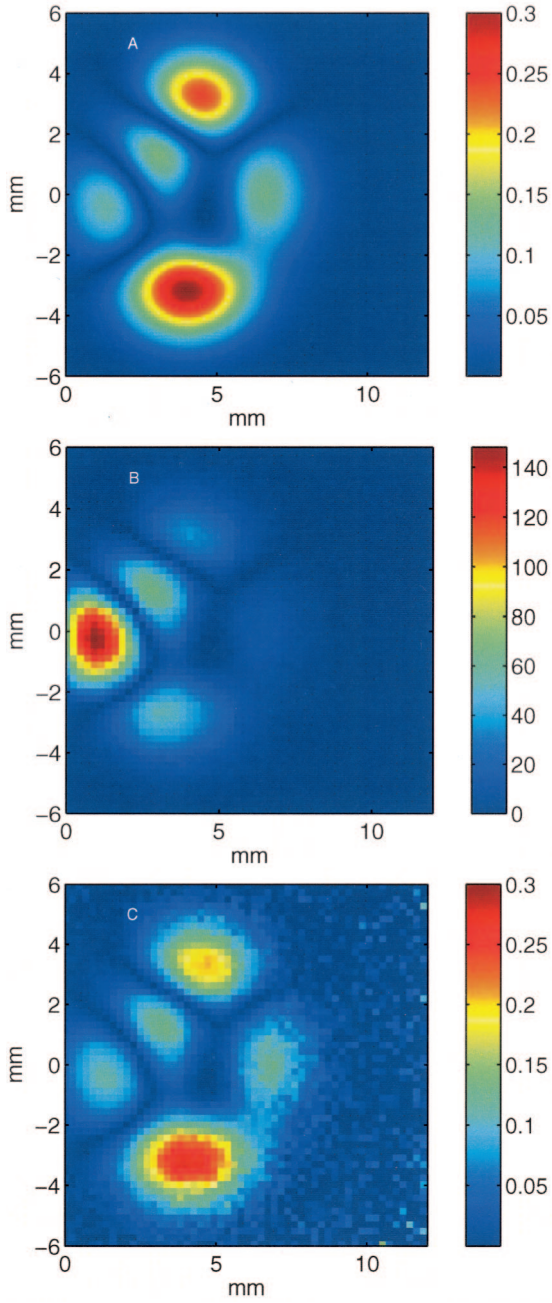

Fig. 5. Quantitative reconstruction of a smoothly varying absorption distribution in a scattering medium. A, true absorption distribution with the absorption coefficient varying smoothly and continuously over space. μ_s = 10 mm^{-1}, g = 0.8, σ = 1. B, measured absorbed energy distribution, in millijoules per cubic centimeter, simulated with a FE model. The SNR ranges from 40 to −40 dB. C, recovered absorption distribution, in inverse millimeters, following 20 iterations.

necessary to have the estimate of the absorption coefficient in absolute units to determine this concentration.

The quantitative inversion algorithm described here, which does estimate the absorption coefficient in absolute units, assumes that the map of absorbed energy density has been recovered accurately, and without significant structural distortion, from the acoustic measurements. In practice this requires a calibrated imaging system with a pointlike point-spread function. Both parts of a PA imaging system, the array of acoustic detectors and the algorithm to backproject the pressure time series to obtain the absorbed energy map, contribute to the point-spread function. A realistic approximation to an ideal reconstruction can be obtained by use of a closely spaced

array of broadband detectors over as great a solid angle as possible, with the assumption that the medium is acoustically homogeneous. These assumptions have been shown to be reasonable through experimental demonstrations in phantoms[3,25] and *in vivo*,[26,27] where good reconstructions of the blood vessel structure on a rodent brain have been obtained by measuring all around, and through, the intact skull.[28,29] Where the image is distorted by the response of the ultrasound detectors or a limited measurement aperture, standard deconvolution routines may be used to improve it.

Although in principle, with the scattering known *a priori*, the absorption coefficient distribution could be recovered from an uncalibrated absorbed energy map, because the shape of the absorbed energy map alone still depends uniquely on the absorption, the recursive algorithm described here requires that the absorbed energy map be calibrated. In principle, this may be achieved with calibrated ultrasound sensors, although further unknowns, such as acoustic coupling, may arise in practice. One may overcome these issues by calibrating the whole system at once, by imaging a phantom of known optical coefficients (perhaps a specific chromophore within the tissue), and comparing the image to the absorbed energy density predicted by an accurate model of light transport within the phantom, such as described in Subsection 3.A. This type of calibration, using a homogeneous absorber, has been used in diffuse optical imaging.[30]

6. Summary

An iterative inversion algorithm that can accurately recover distributions of physiologically realistic optical absorption coefficients from given distributions of absorbed optical energy has been described. It has been shown, by use of simulated examples, that the absorption distribution can be recovered quickly and accurately from the absorbed energy density when the scattering is known. The inversion is robust to noise in the absorbed energy map where the fluence is sufficiently high and any arbitrary pattern of absorption can be recovered.

This work was supported by the Engineering and Physical Sciences Research Council (UK) and the Swiss National Science Foundation.

References

1. K. P. Köstli, M. Frenz, H. Bebie, and H. P. Weber, "Temporal backward projection of optoacoustic pressure transients using Fourier transform methods," Phys. Med. Biol. **46,** 1863–1872 (2001).
2. M. H. Xu, Y. Xu, and L. H. V. Wang, "Time-domain reconstruction-algorithms and numerical simulations for thermoacoustic tomography in various geometries," IEEE Trans. Biomed. Eng. **50,** 1086–1099 (2003).
3. K. Köstli and P. Beard, "Two-dimensional photoacoustic imaging by use of Fourier-transform image: reconstruction and a detector with an anisotropic response," Appl. Opt. **42,** 1899–1908 (2003).
4. J. Laufer, C. Elwell, D. Delpy, and P. Beard, "Pulsed near-infrared photoacoustic spectroscopy of blood," Proc. SPIE **5320,** 57–68 (2004).
5. J. G. Laufer, C. Elwell, D. Delpy, and P. Beard, "*In vitro* measurements of absolute blood oxygen saturation using pulsed near-infrared photoacoustic spectroscopy: accuracy and resolution," Phys. Med. Biol. **50,** 4409–4428 (2005).
6. J. Laufer, C. Elwell, D. Delpy, and P. Beard, "Spatially resolved blood oxygenation measurements using time-resolved photoacoustic spectroscopy," in *Oxygen Transport to Tissue XXVII,* Vol. 578 of Advances in Experimental Medicine and Biology, G. Cicco, D. F. Bruley, M. Ferrari, and D. K. Harrison, eds. (Springer, 2006).
7. R. Kruger, W. Kiser, D. Reinecke, G. Kruger, and K. Miller, "Thermoacoustic optical molecular imaging of small animals," Mol. Imaging **2,** 113–123 (2003).
8. A. A. Karabutov, N. B. Podymova, and V. S. Letokhov, "Time-resolved laser optoacoustic tomography of inhomogeneous media," Appl. Phys. B **63,** 545–563 (1996).
9. G. Paltauf and H. Schmidt-Kloiber, "Pulsed optoacoustic characterization of layered media," J. Appl. Phys. **88,** 1624–1631 (2000).
10. M. Jaeger, J. Niederhauser, M. Hejazi, and M. Frenz, "Diffraction-free acoustic detection for optoacoustic depth profiling of tissue using an optically transparent polyvinylidene flouride pressure transducer operated in backward and forward mode," J. Biomed. Opt. **10,** 024035 (2005).
11. J. Ripoll and V. Ntziachristos, "Quantitative point source photoacoustic inversion formulas for scattering and absorbing media," Phys. Rev. E **71,** 031912 (2005).
12. G. J. Diebold and T. Sun, "Properties of photoacoustic waves in one, two, and three dimensions," Acustica **80,** 339–351 (1994).
13. B. T. Cox and P. C. Beard, "Fast calculation of pulsed photoacoustic fields in fluids using k-space methods," J. Acoust. Soc. Am. **117,** 3616–3627 (2005).
14. G. Paltauf and P. E. Dyer, "Photomechanical processes and effects in ablation," *Chem. Rev.* **103,** 487–518 (2003).
15. Y. V. Zhulina, "Optimal statistical approach to optoacoustic image reconstruction," Appl. Opt. **39,** 5971–5977 (2000).
16. J. Zhang, M. A. Anastasio, X. Pan, and L. V. Wang, "Weighted expectation maximization reconstruction algorithms for thermoacoustic tomography," IEEE Trans. Med. Imaging **24,** 817–820 (2005).
17. S. L. Jacques and L. Wang, "Monte Carlo modeling of light transport in tissues," in *Optical-Thermal Response of Laser-Irradiated Tissue,* A. J. Welch and M. J. C. van Gemert, eds. (Plenum, 1995).
18. S. Arridge, M. Schweiger, M. Hiraoka, and D. Delpy, "A finite element approach for modelling photon transport in tissue," Med. Phys. **20,** 299–309 (1993).
19. M. Schweiger, S. Arridge, M. Hiraoka, and D. Delpy, "The finite element method for the propagation of light in scattering media: boundary and source conditions," Med. Phys. **22,** 1779–1792 (1995).
20. W. M. Star, "Diffusion theory of light transport," in *Optical-Thermal Response of Laser-Irradiated Tissue,* A. J. Welch and M. J. C. van Gemert, eds. (Plenum, 1995).
21. S. R. Arridge and W. R. B. Lionheart, "Nonuniqueness in diffusion-based optical tomography," Opt. Lett. **23,** 882–884 (1998).
22. M. O'Leary, D. Boas, B. Chance, and A. Yodh, "Experimental images of heterogeneous turbid media by frequency-domain diffusing-photon tomography," Opt. Lett. **20,** 426–428 (1995).
23. B. T. Cox, S. Arridge, K. Köstli, and P. Beard, "Quantitative photoacoustic imaging: fitting a model of light transport to the initial pressure distribution," Proc. SPIE **5697,** 49–55 (2005).
24. R. Aster, B. Borchers, and C. Thurber, *Parameter Estimation and Inverse Problems* (Elsevier, 2005).

25. C. G. A. Hoelen, F. F. M. de Mul, R. Pongers, and A. Dekker, "Three-dimensional photoacoustic imaging of blood vessels in tissue," Opt. Lett. **23,** 648– 650 (1998).
26. R. A. Kruger, K. D. Miller, H. E. Reynolds, W. L. Kiser, D. R. Reinecke, and G. A. Kruger, "Contrast enhancement of breast cancer *in vivo* using thermoacoustic ct at 434 MHz—feasibility study," Radiology **216,** 279–283 (2000).
27. R. I. Siphanto, R. G. M. Kolkman, A. Huisjes, M. C. Pilatou, F. F. M. de Mul, W. Steenbergen, and L. N. A. van Adrichem, "Imaging of small vessels using photoacoustics: an *in vivo* study," Lasers Surg. Med. **35,** 354–362 (2004).
28. X. Wang, Y. Pang, G. Ku, X. Xie, G. Stoica, and L. V. Wang, "Noninvasive laser-induced photoacoustic tomography for structural and functional *in vivo* imaging of the brain," Nat. Biotechnol. **21,** 803–806 (2003).
29. X. Wang, Y. Pang, G. Ku, G. Stoica, and L. V. Wang, "Three-dimensional laser-induced photoacoustic tomography of mouse brain with the skin and skull intact," Opt. Lett. **28,** 1739–1741 (2003).
30. H. Jiang, K. Paulsen, and U. Oesterberg, "Optical image reconstruction using dc data simulations and experiments," Phys. Med. Biol. **41,** 1483–1498 (1996).